# Device physics of colloidal quantum dot solar cells

Speirs, Mark Jonathan

# 5 P-type doping of thiol-capped PbS films


## Abstract

*Lead sulfide quantum dot (PbS QD) solar cell efficiencies have improved rapidly over the past years due in large part to intelligent band alignment considerations. A pn-junction can be formed by connecting PbS layers with contrasting ligands. However, the resulting doping concentrations are typically low and can not be effectively controlled. Here, we present a method of chemically p-doping films of thiol capped PbS QDs. P-n junction solar cells with increased doping in the p-type layer show improved short circuit current and fill factor, leading to an improvement in the power conversion efficiency from 7.1% to 7.6%. By examining Schottky diodes and the absorption spectra of treated and untreated PbS QDs, we show that the improved efficiency is due to the increased doping concentration in the thiol capped QD layer and to denser packing of the PbS QD film.*



*Submitted as:*

M. J. Speirs, D. M. Balazs, D. Dirin, M. Kovalenko, M. A. Loi, Increased efficiency in pn-junction PbS QD solar cells via NaHS treatment of the p-type layer, *Appl. Phys. Lett.*,

## 5.1 Introduction

For the past decade, lead sulfide quantum dots (PbS QDs) have been a topic of great interest in the field of solution-processable photovoltaics.[1] Their success stems in part from the large (18 nm) Bohr radius of PbS,[2] which leads to a broadly tunable bandgap for QDs in the size range 3-5 nm, and in part from the electronic adaptability offered by the large library of ligands able to modify the QD surface. This not only allows control over charge carrier mobility, but also allows control of the conduction and valence levels with respect to the vacuum level, as well as the position of the Fermi energy level within the bandgap.[3] Clever implementation of these versatile characteristics has driven the steady increase in power conversion efficiency (*PCE*) to more than 11% to date.[4] The most efficient device structures currently feature a junction between an n-type layer of PbS, treated with tetrabutylammonium iodide (TBAI), and a layer of EDT-capped PbS.[5–7] The alignment of the Fermi levels across the junction gives rise to a built in electric field which induces beneficial band-bending and facilitates drift driven charge extraction.[7]

Nevertheless, PbS QD solar cells still fall well short of their potential, in particular due to a low fill factor (*FF*), and an open circuit voltage ($V_{OC}$) that falls well below the theoretical limit.[8,9] In the previous chapter, we demonstrated that these solar cells can benefit from an increased doping concentration in the EDT layer.[7] Due to charge conservation across the p-n junction, the distribution of the depletion region across the junction is governed by

$$N_D w_n = N_A w_p \tag{5.1}$$

with $N_{D(A)}$ the doping concentration of of the n(p)-type layer and $w_{D(A)}$ the fraction of the depletion region located on the n(p)-type side. Thus, increased doping in the EDT layer would shift the distribution of the depletion region towards the TBAI layer, which has higher charge carrier mobility,[7] and would thus facilitate more efficient charge extraction.

Many doping strategies have been demonstrated for lead chalcogenide QDs.[10] These include doping via oxidation,[11–16] ligand control,[3,13,17,18] stoichiometry and defects,[19–21] dipoles,[22] and heterovalent impurities.[23–25] While n-type films have been fabricated through ligands such as hydrazine and halide salts,[18,26] p-type doping of thiol-capped films has so far mostly been achieved via oxidation in ambient conditions. That doping strategy has

been used explicitly by Choi et al. in Schottky solar cells,[15] and implicitly in p-n junction devices which have been exposed to air during or after deposition of the thiol-capped layer.[6,27] Chuang et al. reported that p-n junction devices stored in air can display an initial increase in efficiency, which can be attributed to the increased doping of the EDT-capped layer.[6] Nevertheless, oxidative doping is not well controlled, and while oxygen is effective in shifting the Fermi level, the unavoidable adsorption of other atmospheric contaminants, in particular water, onto the PbS surface is likely to have a detrimental effect on trap densities and charge carrier mobilities. Therefore, a more controlled and systematic method of p-doping is desirable. Instead, control of the stoichiometry of lead chalcogenide QDs has been proposed as a controllable method of tuning the Fermi level in lead chalcogenide QDs.[21] Oh et al. showed that thermally evaporating excess Pb onto PbSe QD films enhances the n-type behaviour and, similarly, more p-type behaviour was achieved by evaporating excess Se.[19] However, this method is difficult to control, and might lead to unstable film properties due to the diffusion of the evaporated atoms. Furthermore, it is desirable to achieve the doping via solution-processable techniques, compatible with cheap and large scale production methods. Oh et al. also reported an increase in solar cell efficiency using a combination of SCN and BDT ligands.[28] In that work, the solar cells treated with both BDT and SCN exhibited a modest efficiency of 3.5%, compared to 2.1% for solar cells's treated with only BDT. It was also noted that this method was limited to active layers less than 150 nm thick, as the poor resulting mobility hinders charge extraction in thicker films. Chalcogenide salts such as $Na_2S$, $Na_2Se$ and $K_2S$ are soluble in polar solvent and have been demonstrated to effectively alter the PbS, PbSe or CdSe stoichiometry and increase p-type doping in transistors, leading to higher p-type currents and charge carrier mobility in field effect transistors.[28–32] However, the success of these salts in solar cell structures has been limited, likely due to the extremely high reactivity of these salt which can introduce trap states into the film and cause pronounced fusion of the QDs, leading to a lower $V_{OC}$.

In this chapter, we fabricate efficient p-n junction solar cells using TBAI treated PbS as n-type layer and EDT-capped PbS as p-type layer. We report a simple and reproducible method of p-doping thiol-capped PbS films by post deposition treatment with a solution of sodium hydrosulfide (NaHS), and show an increase of the short circuit current ($J_{SC}$) and $FF$ for p-n junction QD solar cells without detriment to the $V_{OC}$, leading to an improvement of the

*PCE* from 7.1% to 7.6%.

We fabricate Schottky diodes with various concentrations of doping. The doping concentration is measured via Mott-Schottky analysis and found to increase by more than a factor of three. Under illumination, decreasing $J_{SC}$ of the Schottky devices is observed with increasing doping concentration, which can be explained by a narrowing of the depletion region near the Schottky junction due to increased doping. We see no change in the $V_{OC}$ or *FF*, indicating that the doping procedure has little effect on charge transport properties or recombination rates. Finally, the absorption spectra reveal only a very small loss in quantum confinement upon NaHS treatment.

# Results and Discussion

## 5.1.1 Doped p-n junction solar cells

PbS QDs capped with oleic acid are synthesized using an adaptation of a previously reported method.[33] A compact film of anatase $TiO_2$ is prepared by spincoating a 20 : 2 : 1 solution of ethanol : titanium(IV) butoxide : HCl onto pre-patterned fluorine doped tin-oxide substrates (13 Ω/sq) and annealed at 450 °C for 30 minutes. The n-type PbS film is deposited by the layer-by-layer spincoating of a 10 mg/ml solution of PbS in hexane, followed by exposure of the film to 15 mg/ml TBAI in methanol, subsequent spin-drying and finally, two washing steps with pure methanol to remove the tetrabutylammonium cation. The p-type layer is formed by spincoating of the oleic acid-capped PbS QDs, followed by exposure of the film to a 0.01% $^{v}/_{v}$ EDT in acetonitrile and one washing step with pure acetonitrile. For the doped samples, each EDT-treated layer was exposed to a 0.1 mM solution of NaHS in MeOH for 15 s after the EDT treatment and prior to the washing step. We observe that higher concentrations of NaHS often led to delamination of the active layer. The active layer comprises 12 layers (∼200 nm) of TBAI and 4 layers (∼60 nm) of EDT-capped PbS. Since some degree of oxidative doping is unavoidable, we choose to expose all devices to air prior to deposition of the electrodes to ensure that any effect we see is in addition to the oxidative doping.

The devices are finished by thermal evaporation of 5 nm $MoO_3$ and 80 nm of Au. Here we would like to comment on the use of $MoO_3$ as a hole extracting layer, since there are conflicting reports concerning the use of $MoO_3$

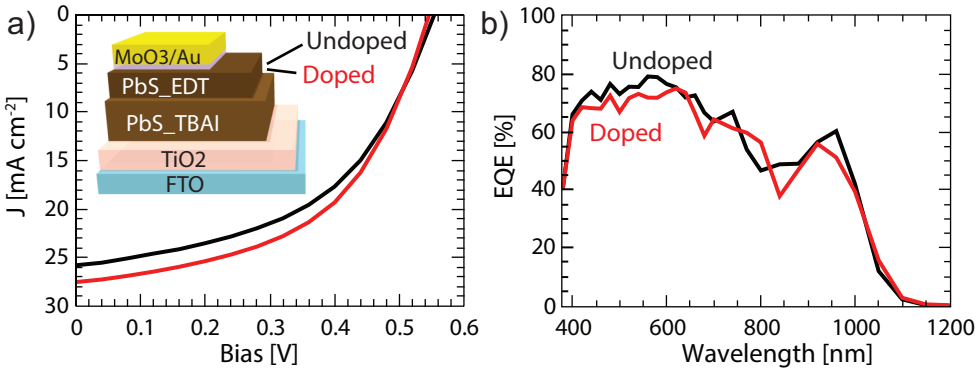


**Figure 5.1.** a) Representative *J-V* curves of p-n junction solar cell doped with 0.1 mM NaHS in MeOH (red) and undoped (black) PbS_ EDT layers. The device structure is shown in the inset. b) External quantum efficiency of p-n juntion PbS QD solar cells, with undoped and doped PbS_ EDT layer.

in the literature. Some authors have reported high efficiencies using only Au as a top electrode,[5,6] and report a decreased stability when $MoO_3$ is used.[6] Other studies choose to include $MoO_3$ as part of the anode,[34–36] and Hu et al. have reported that a detrimental Schottky barrier is formed at the PbS/Au interface,[37] which can be removed by using $MoO_3$ as an interlayer.[38] In our case, devices without $MoO_3$ have an impractically low yield of non-shorted devices, possibly due to the penetration of Au clusters into the active layer during thermal deposition, which the $MoO_3$ is able to prevent. Therefore we have chosen to include $MoO_3$ both as a hole transporting layer and as protection for the active layer from the electrode deposition.

The current-voltage (*J-V*) curves of representative doped and undoped devices are shown in Figure 5.1a and the main figures of merit are shown in Table 5.1.

In total, 13 devices on 4 independent substrates were made for the undoped case and 11 devices over 4 substrates for the doped case. To avoid the

**Table 5.1.** *J-V* figures of merit with doped and undoped PbS_EDT layers. The values in brackets give the standard deviation over the data set.

| Device | $J_{SC}$ [mA/cm$^2$] | $V_{OC}$ [V] | *FF* | *PCE* [%] |
|---|---|---|---|---|
| Best undoped | 26.4 | 0.56 | 0.53 | 8.1 |
| Best doped | 27.4 | 0.55 | 0.56 | 8.6 |
| Undoped average | 26.0($\pm$0.8) | 0.56($\pm$0.01) | 0.49($\pm$0.02) | 7.1($\pm$0.6) |
| Doped average | 27.0($\pm$ 0.4) | 0.55($\pm$ 0.01) | 0.51($\pm$ 0.03) | 7.6($\pm$ 0.6) |

inclusion of shorted or almost shorted devices, only solar cells with a high rectification ratio in the dark ($J_{|V=1}/J_{|V=-1} > 100$) were included in the dataset. The doped solar cells show small but consistent increases in $J_{SC}$, from 26.0 to 27.0 mA/cm$^2$, and $FF$, from 0.49 to 0.51, with a practically unchanged $V_{OC}$, leading to an average increase in $PCE$ from 7.1% to 7.6%, and an increase of the highest values from 8.1% to 8.6%. The external quantum efficiency ($EQE$) spectra are shown in Figure S1; the current calculated by integrating the product of the $EQE$ spectrum with the AM1.5G solar spectrum corresponds well to the current obtained in the $J$-$V$ curves.

### 5.1.2 Schottky diode analysis

To determine the reason for this improvement, the PbS_EDT layer is examined independently. To this end Schottky diodes are fabricated by depositing 150-180 nm PbS_EDT on pre-patterned indium tin oxide (ITO) and finished with 1 nm of LiF and 100 nm aluminium. The parallel plate capacitance $C$ is measured as a function of bias in the dark; a 25 mV ac signal with frequency 250 Hz was superimposed on a forward bias ranging from -0.5 V to 0.5 V. The resulting $C-V$ plots are shown in Figure 5.2. The doping concentration

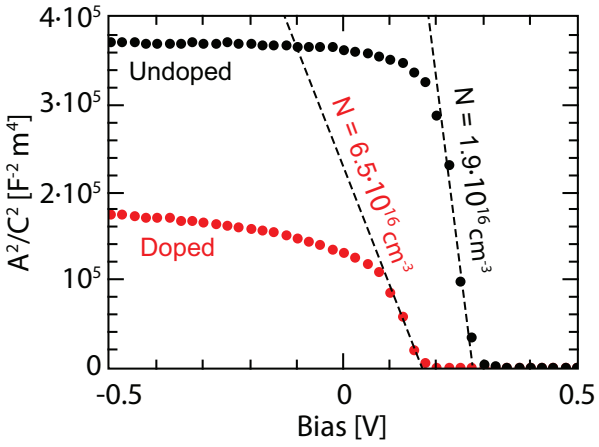


**Figure 5.2.** Voltage dependent capacitance extracted from impedance spectra in the dark for doped (red) and undoped (black) PBS_EDT.

$N$ can be obtained using the the Mott-Schottky equation,

$$\frac{A^2}{C^2} = \frac{2}{q\varepsilon_r\varepsilon_0 N}\left(V - V_{bi} - \frac{kT}{q}\right) \tag{5.2}$$

where $A$ is the device area, $\varepsilon_r$ and $\varepsilon_0$ are the relative and vacuum permittivity, respectively, $V_{bi}$ is the built in voltage, $k$ is Boltzmann's constant, $T$ is the temperature, and $e$ is the elementary charge. In the voltage range where the depletion region depends on the applied bias, the Mott-Schottky curve is linear, and a doping concentration of $1.9{\cdot}10^{16}$ cm$^{-3}$ is found for the undoped film, while the film doped with NaHS shows a more than threefold higher doping concentration of $6.5{\cdot}10^{16}$ cm$^{-3}$. In light of this, the $V_{OC}$ of these solar cells is expected to increase by approximately 28 mV due to increased built in bias over the pn-junction according to

$$V_{bi} = \frac{kT}{q} \ln\left(\frac{N_A N_D}{n_i^2}\right). \tag{5.3}$$

Since this increase is not observed, it must be negated by either increased charge carrier recombination or a lower bandgap.

The charge carrier lifetime plays a crucial role in the device performance. Increasing the density of states within the bandgap can potentially assist detrimental recombination processes leading to a reduced charge carrier lifetime. To elucidate the role this doping method has on the recombination rates of minority charge carriers, in this case electrons, impedance spectra were obtained while holding the diodes at open circuit bias under 1 Sun illumination. Since no current flows through the device at open circuit bias, all photogenerated charge carriers must necessarily recombine. The typical rate at which the recombination takes place can be found from $\tau = R_r C_r$,[39] where $R_r$ is the recombination resistance and $C_r$ is the capacitance found by fitting the Nyquist plots with the equivalent circuit consisting of a constant phase element (Q) in parallel with the recombination resistance and a series resistance, see the inset in Figure 5.3. The constant phase element takes into account the slightly depressed impedance spectra, which can be explained by small inhomogeneities such as roughness or pinholes at the electrode interface.[40] The fitting parameter $a$ indicating the deviation from an ideal capacitor is 0.96 for these devices, indicating almost ideal capacitance behaviour. The capacitance is calculated from the constant phase element using the relationship $C_{eq} = Q\left(2\pi f_{peak}\right)^{a-1}$,[41] where $f_{peak}$ is the frequency at the peak maximum imaginary component of the Nyquist spectrum. With this method, carrier lifetimes of 5.4 $\pm$ 1.1 $\mu$s for the undoped film and an almost equal 4.2 $\pm$ 0.9 $\mu$s for the film doped with NaHS. These values are comparable to the values obtained by the alternative method which uses the equation $\tau = 1/\left(2\pi f_{peak}\right)$,[39]

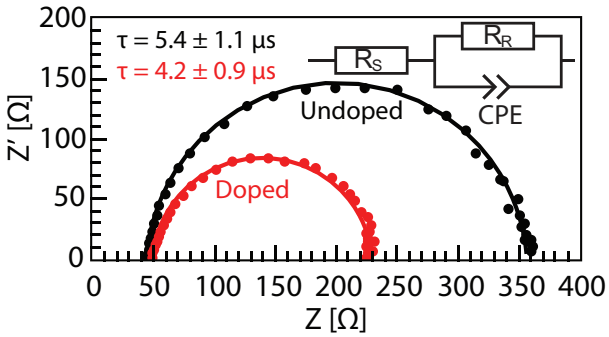


**Figure 5.3.** Nyquist impedance spectra of doped and undoped films under 1 Sun illumination, held at open circuit voltage.

which gives values of 5.0 $\pm$ 0.6 $\mu$s for the undoped film and 4.4 $\pm$ 0.5 $\mu$s for the doped film. The close similarity in lifetimes indicates that the doping process does not affect the recombination rates under normal operating conditions.

*J-V* curves of three Schottky diodes fabricated with NaHS concentrations of 0, 0.02, and 0.1 mM were measured under 1 Sun illumination to further investigate the effect of NaHS doping on the properties of PbS_EDT films. The curves are shown in Figure 5.4, and the solar cell parameters are shown in Table 5.2. In contrast to the p-n junction solar cells, the $J_{SC}$ of these devices decreases with increasing doping, while the $V_{OC}$ and $FF$ are both unchanged. Charge extraction in Schottky solar cells is limited by diffusion of the charge carriers towards the Schottky barrier,[42] in this case the aluminium contact, where energy level bending drives the separation of electrons and holes to their respective electrodes. For a Schottky junction, the width of the depletion region is given by[43]

$$w = \left[\frac{2\varepsilon_0\varepsilon_r}{qN}\left(V_{bi} - V - \frac{kT}{q}\right)\right]^{1/2}, \tag{5.4}$$

**Table 5.2.** *J-V* figures of merit of Schottky devices with doped and undoped PbS_EDT layers.

| Device | $J_{SC}$ [mA/cm$^2$] | $V_{OC}$ [V] | $FF$ | $PCE$ [%] |
|---|---|---|---|---|
| Undoped | 9.1 | 0.42 | 0.56 | 2.3 |
| 0.02 mM NaHS | 6.4 | 0.41 | 0.54 | 1.4 |
| 0.1 mM NaHS | 4.8 | 0.41 | 0.54 | 1.1 |

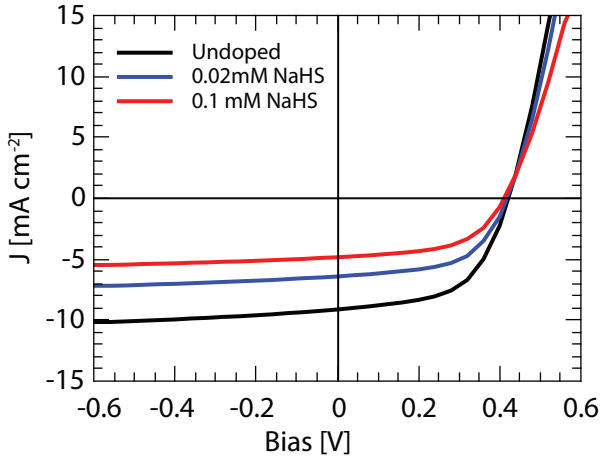


**Figure 5.4.** *J-V* curves for Schottky solar cells exposed to 0.1 mM NaHs (red), 0.02 mM NaHS (blue) and without additional doping (black).

thus the decreasing $J_{SC}$ can be attributed to the narrowing of the depletion region, caused by the increased doping concentration $N$. The constant $V_{OC}$ is another indication that the doping mechanism does not significantly alter the trap density or charge carrier lifetimes, while the unchanged $FF$ indicates that the doping mechanism does not significantly improve or impair charge extraction.

The ideality factor $n$ was then calculated from the dependence of the $V_{OC}$ on the light intensity ($I$) (Figure 5.5)

$$V_{OC} = \frac{nkT}{q} \ln\left(\frac{J_{PH}}{J_0}\right) \tag{5.5a}$$

$$= \frac{nkT\alpha}{q} \ln(I) + c \tag{5.5b}$$

where $k$ is Boltzmann's constant, $T$ is the temperature, $e$ is the elementary charge, $\alpha$ is an empirical parameter indicating the linearity of the photocurrent with intensity ($J_{PH} \propto I^{\alpha}$), and $c$ is a fitting parameter collecting all the terms independent of light intensity.

For the undoped films an ideality factor of 1.50 is found, while for the doped film a similar value of 1.57 is found. An ideality factor of 1 corresponds to fully bimolecular recombination, while an ideality factor of 2 means that trap assisted recombination is the dominating mechanism. The similar values of $n$ measured for the doped and undoped films confirms that NaHS does

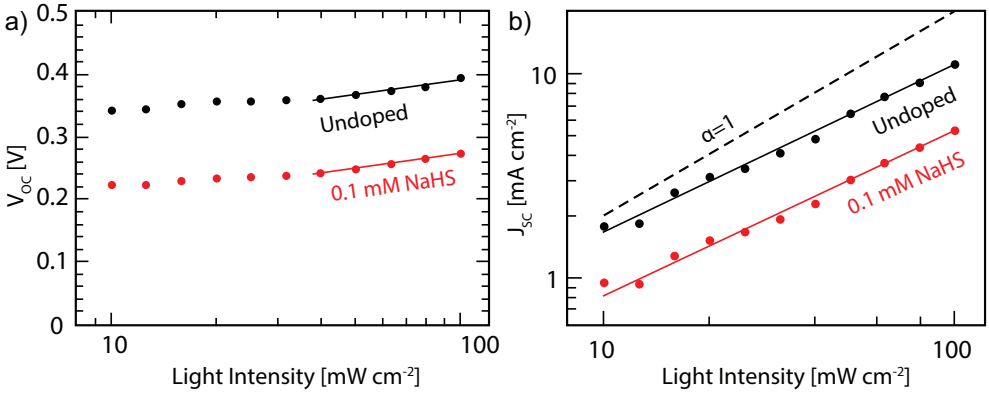


**Figure 5.5.** a) Light intensity dependence of the $V_{OC}$ for undoped (black dots) and doped with 0.1 mM of NaHS solution (red dots). The solid lines represent the best fit of the slopes from which the ideality factor is calculated. b) Light intensity dependence of the $J_{SC}$. The dashed line represents ideal linear photocurrent behaviour.

not introduce a significant amount of traps or alter the main recombination processes.

Finally, from the absorption spectrum in Figure 5.6, we see a small redshift of the treated QDs from 915 nm to 940 nm, corresponding to a difference in bandgap of 36 meV, which could indicate slightly denser packing, leading to partial loss of quantum confinement coupled with higher film conductivity. The decrease of the bandgap is close to the 28 meV increase in $V_{OC}$ expected from a threefold increase in the p-type doping concentration. Additionally, we observe a beneficial increase of the absorption coefficient. Though this effect is present to some degree in our films, its influence is small since we do not see a decrease in the $V_{OC}$ of the solar cells. Similarly, if this was the dominant effect we would expect to see increased $J_{SC}$ in the Schottky devices. Instead, the Schottky devices are dominated by the decreased depletion width caused by higher doping.

In conclusion, we have demonstrated a method to increase the p-type doping concentration of EDT capped PbS QD films, without degrading any other properties. In efficient pn-junction solar cells we have shown an improvement in both $J_{SC}$ and FF, without degradation of the $V_{OC}$, leading to an average performance improvement of 0.5 percentage points. We have shown that this doping mechanism does not significantly change the charge carrier lifetime, and that the change in $J_{SC}$ and FF is due to both the increase in doping concentration by a factor of three, which shifts the depletion region towards the TBAI

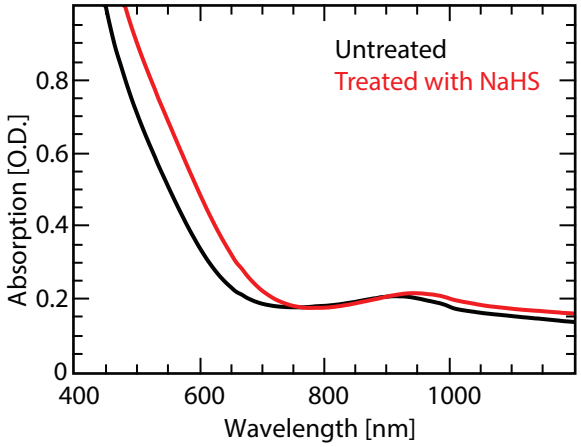


**Figure 5.6.** Absorption spectrum of untreated (black) and NaHS treated (red) PbS QD films

capped PbS layer, and due to the higher absorption coefficient and possibly higher film conductivity. The expected increase in $V_{OC}$ from the increased doping is compensated by the slight loss of quantum confinement after NaHS treatment. We would like to note that an even higher doping concentration would be desirable to further decrease the necessary thickness of the p-type layer, similar to the strategy used in many silicon solar cells, where a thick low doping concentration (usually p-type) layer is used in combination with a thin highly doped (n-type) layer. In this case we were limited by the mechanical stability of our active layer, which exhibited frequent delamination when exposed to higher concentrations of NaHS in methanol. Further increasing the doping concentration of the p-type layer is expected to yield even better results.

# Conclusion

In conclusion, we have demonstrated a method to increase the p-type doping concentration of EDT-capped PbS QD films, without degrading any other properties. In efficient p-n junction solar cells we have shown an improvement in both $J_{SC}$ and $FF$, without degradation of the $V_{OC}$, leading to an average performance improvement of 0.5 percentage points from 7.1% to 7.6%. We have shown that this doping mechanism does not significantly change charge carrier mobility, trap density, or recombination rates, so the change in

device performance is solely due to the increase in doping concentration by a factor of three, which shifts the depletion region towards the TBAI treated layer, improving current extraction and fill factor. We would like to note that an even higher doping concentration would be desirable to further decrease the necessary thickness of the p-type layer, similar to the strategy used in many silicon solar cells, where a low doping concentration (usually n-type) layer is used in combination with a highly doped (p-type) layer. In this case we were limited by the mechanical stability of our active layer, which exhibited frequent delamination when exposed to higher concentrations of NaHS in methanol. Further increasing the doping concentration of the p-type layer is expected to yield even better results.

## 5.2 Experimental Details

**Nanocrystal synthesis.** Lead sulfide quantum dots (PbS QDs) were synthesized using the ubiquitous hot injection method.[33] In short, a 2 mmol solution of $Pb(CH_3COO)_2 \cdot 3H_2O$, octadecane (ODE) and oleic acid (ratio 1:1) in a three-neck flaskwere held under vacuum at 100 °C for 2 hours to dissolve the lead salt and dry the solution, after which the temperature is raised to 145 °C. The sulfur precursor solution consisting of 1 mmol bis(trimethylsilyl) sulfide in ODE was prepared in inert atmosphere and quickly injected into the flask, after which the flask is cooled to room temperature with a water bath. The QDs are then washed in a mixture of hexane (20 ml) and ethanol (40 ml) and centrifuged to separate out the QDs. This process is repeated 3 times, and finally the QDs are redispersed into hexane.

**Device preparation.** Solar cells were fabricated on top of pre-patterned fluorine doped tin oxide substrates (Visiontek Products, 13 Ω/sq). The substrates were scrubbed using a textured glove and soapy water, rinsed with deionized water, sonicated in acetone and isopropyl alcohol for 10 minutes and dried in an oven. Shortly before deposition of the $TiO_2$, the substrate was subjected to an $O_2$-rich plasma treatment for 30 s. To form the $TiO_2$ layer a solution of titanium butoxide, 37% HCl in ethanol, and pure ethanol in ratio 2:1:20 was spincoated at a rate of 4000 rpm and annealed at 450 C for 30 mins, followed by a slow cool-down to room temperature. The PbS film was depositied in a $N_2$ filled glovebox using a layer-by-layer method whereby a 10

mg/ml solution of PbS in hexane is spincasted at a rate of 1000 rpm. The film is then exposed to the ligand solution for 30 s, follwed by one or more washing steps and spin drying. This process is repeated untill the desired thickness is achieved. For the n-type layer, a ligand solution of 15 mg/ml tetrabutylammonium iodide in methanol is used, follwed by two washing steps with pure methanol, while for the p-type layer a solution of ethanedithiol (EDT) in acetonitril (0.01% $^{v}/_{v}$) with one washing step using pure acetonitrile. For the doped layers, the EDT-capped film is exposed to a 0.1 mM solution of sodium hydrosulfide for 15 s prior to the washing step. Twelve layers of TBAI and four layers of EDT were used to form a total thickness of approximately 280 nm. The samples were then brought into ambient atmosphere for 10 minutes before thermal evaporation of 5 nm of molybdenum trioxide at a rate of 0.2 Å/s, and 80 nm of gold at a rate of 0.5 -2 Å/s.

For the fabrication of Schottky diodes, poly(3,4-ethylenedioxythiophene)-poly(styrenesulfonate) (PEDOT:PSS) was deposited onto pre patterned indium tin oxide subtrates (13 Ω/s) at 500 rpm. The active was formed by 10 layers of PbS deposited with the same method as the solar cells, and exposed to ambient air befor deposition of 1 nm LiF and 100 nm aluminium.

**Device measurements.** *J-V* sweeps were carried out in inert environment using a Keithley 2400 source-meter. Simulated AM1.5G illumination was provided by a Steuernagel Solarconstant 1200 metal halide lamp set to 100 mW/cm$^2$ intensity, measured by a silicon reference cell (SRC-1000-RTD-QZ, VLSI Standards Inc.) and corrected for the spectral mismatch. The illuminated area was limited to 0.10 cm$^2$ by a well defined shadow mask for efficiency calculations. The temperature was controled by an adjustable $N_2$ gas flow through a liquid $N_2$ bath.

Mott-Schottky curves were measured using a SP-200 Bio-Logic potentiostat. A forward bias ranging from -0.5 V to 0.5 V is superimposed with a 20 mV AC pertubation with a frequency of 250 Hz. For carrier lifetime measurements, the device is held at open circuit bias under 1 Sun illumination while impedance spectra are measured over the frequency range 1 MHz to 100 Hz.

# References


[1] M. V. Kovalenko, *Nat. Nanotechnol.* **2015**, *10*, 994–997.

[2] F. Wise, *Acc. Chem. Res.* **2000**, *33*, 773–780.

[3] P. R. Brown, D. Kim, R. R. Lunt, N. Zhao, M. G. Bawendi, J. C. Grossman, V. Bulović, *ACS Nano* **2014**, *8*, 5863.

[4] M. Liu, O. Voznyy, R. F. Sabatini, P. García de Arquer, R. Munir, A. H. Balawi, X. Lan, F. Fan, G. Walters, A. R. Kirmani, S. Hoogland, F. Laquai, A. Amassian, E. H. Sargent, *Nat. Mater.* **2016**.

[5] X. Lan, O. Voznyy, F. P. Garcia de Arquer, M. Liu, J. Xu, A. H. Proppe, G. Walters, F. Fan, H. Tan, M. Liu, Z. Yang, S. E. H., *Nano Lett.* **2016**, DOI: 10.1021/acs.nanolett.6b01957.

[6] C.-H. M. Chuang, P. R. Brown, V. Bulović, V., M. G. Bawendi, *Nat. Mater.* **2014**, *13*, 796.

[7] M. J. Speirs, D. N. Dirin, M. Abdu-Aguye, D. M. Balazs, M. V. Kovalenko, M. A. Loi, *Energy Environ. Sci.* **2016**, *9*, 2916–2924.

[8] C.-H. M. Chuang, A. Maurano, R. E. Brandt, G. W. Hwang, J. Jean, T. Buonassisi, V. Bulović, M. G. Bawendi, *Nano Lett.* **2015**, *15*, 3286–3294.

[9] A. Polman, M. Knight, E. C. Garnett, B. Ehrler, W. C. Sinke, *Science* **2016**, *352*, DOI: 10.1126/science.aad4424.

[10] A. Stavrinadis, G. Konstantatos, *ChemPhysChem* **2015**, *17*, 632–644.

[11] E. J. Klem, H. Shukla, S. Hinds, D. D. MacNeil, L. Levina, E. H. Sargent, *Appl. Phys. Lett.* **2008**, *92*, 212105.

[12] D. M. Balazs, M. I. Nugraha, S. Z. Bisri, M. Sytnyk, W. Heiss, M. A. Loi, *Appl. Phys. Lett.* **2014**, *104*, 112104.

[13] O. Voznyy, D. Zhitomirsky, P. Stadler, Z. Ning, S. Hoogland, E. H. Sargent, *ACS Nano* **2012**, *6*, 8448–8455.

[14] G. Konstantatos, L. Levina, A. Fischer, E. H. Sargent, *Nano Lett.* **2008**, *8*, 1446–1450.

[15] M.-J. Choi, J. Oh, J.-K. Yoo, J. Choi, D. Sim, Y. S. Jung, *Energy Environ. Sci.* **2014**.

[16] S. J. Oh, C. Uswachoke, T. Zhao, J.-H. Choi, B. T. Diroll, C. B. Murray, C. R. Kagan, *ACS Nano* **2015**, *9*, 7536–7544.

[17] A. H. Ip, S. M. Thon, S. Hoogland, O. Voznyy, D. Zhitomirsky, R. Debnath, L. Levina, L. R. Rollny, G. H. Carey, A. Fischer, K. W. Kemp,

I. J. Kramer, Z. Ning, A. J. Labelle, K. W. Chou, A. Amassian, E. H. Sargent, *Nat. Nano.* **2012**, *7*, 577.
[18] D. Zhitomirsky, M. Furukawa, J. Tang, P. Stadler, S. Hoogland, O. Voznyy, H. Liu, E. H. Sargent, *Adv. Mater.* **Dec. 2012**, *24*, 6181.
[19] S. J. Oh, N. E. Berry, J.-H. Choi, E. A. Gaulding, T. Paik, S.-H. Hong, C. B. Murray, C. R. Kagan, *ACS Nano* **2013**, *7*, 2413–2421.
[20] J. M. Luther, J. M. Pietryga, *ACS Nano* **2013**, *7*, 1845–1849.
[21] D. Kim, D.-H. Kim, J.-H. Lee, J. C. Grossman, *Phys. Rev. Lett.* **2013**, *110*, 196802.
[22] M. I. Nugraha, H. Matsui, S. Z. Bisri, M. Sytnyk, W. Heiss, M. A. Loi, J. Takeya, *APL Mater.* **2016**, *4*, 116105.
[23] J. Liu, Q. Zhao, J.-L. Liu, Y.-S. Wu, Y. Cheng, M.-W. Ji, H.-M. Qian, W.-C. Hao, L.-J. Zhang, X.-J. Wei, S.-G. Wang, J.-T. Zhang, Y. Du, S. X. Dou, H.-S. Zhu, *Adv. Mater.* **2015**, *27*, 2753–2761.
[24] H. Liu, D. Zhitomirsky, S. Hoogland, J. Tang, I. J. Kramer, Z. Ning, E. H. Sargent, *Appl. Phys. Lett.* **2012**, *101*, 151112.
[25] A. Stavrinadis, A. K. Rath, F. P. G. de Arquer, S. L. Diedenhofen, C. Magén, L. Martinez, D. So, G. Konstantatos, *Nat. Commun.* **2013**, *4*.
[26] D. V. Talapin, C. B. Murray, *Science* **2005**, *310*, 86–89.
[27] M. Yuan, O. Voznyy, D. Zhitomirsky, P. Kanjanaboos, E. H. Sargent, *Adv. Mater.* **2015**, *27*, 917–921.
[28] S. Oh, D. Straus, T. Zhao, J.-H. Choi, S.-W. Lee, E. Gaulding, C. Murray, C. Kagan, *Chem. Comm.* **2017**, *53*, 728–731.
[29] E. Goodwin, D. B. Straus, E. A. Gaulding, C. B. Murray, C. R. Kagan, *Chem. Phys.* **2016**, *471*, 81–88.
[30] Y. Liu, J. Tolentino, M. Gibbs, R. Ihly, C. L. Perkins, Y. Liu, N. Crawford, J. C. Hemminger, M. Law, *Nano Lett.* **2013**, *13*, 1578–1587.
[31] D. K. Kim, A. T. Fafarman, B. T. Diroll, S. H. Chan, T. R. Gordon, C. B. Murray, C. R. Kagan, *ACS Nano* **2013**, *7*, 8760–8770.
[32] A. Nag, M. V. Kovalenko, J.-S. Lee, W. Liu, B. Spokoyny, D. V. Talapin, *J. Am. Chem. Soc.* **2011**, *133*, 10612–10620.
[33] M. A. Hines, G. D. Scholes, *Adv. Mater.* **2003**, *15*, 1844–1849.
[34] T. Zhao, E. D. Goodwin, J. Guo, H. Wang, B. T. Diroll, C. B. Murray, C. R. Kagan, *ACS Nano* **2016**, *10*, 9267–9273.
[35] A. Rath, F. P. García de Arquer, A. Stavrinadis, T. Lasanta, M. Bernechea, S. L. Diedenhofen, G. Konstantatos, *Adv. Mater.* **2014**, *26*, 4741.

[36] K. W. Kemp, A. J. Labelle, S. M. Thon, A. H. Ip, I. J. Kramer, S. Hoogland, E. H. Sargent, *Adv. Energy Mater.* **2013**, *3*, 917.

[37] L. Hu, A. Mandelis, X. Lan, A. Melnikov, S. Hoogland, E. H. Sargent, *Sol. Energ. Mat. Sol. Cells* **2016**, *155*, 155–165.

[38] P. R. Brown, R. R. Lunt, N. Zhao, T. P. Osedach, D. D. Wanger, L.-Y. Chang, M. G. Bawendi, V. Bulović, V., *Nano Lett.* **2011**, *11*, 2955–2961.

[39] L.-H. Lai, L. Protesescu, M. V. Kovalenko, M. A. Loi, *Phys. Chem. Chem. Phys* **2014**, *16*, 736.

[40] B. Hirschorn, M. E. Orazem, B. Tribollet, V. Vivier, I. Frateur, M. Musiani, *Electrochim. Acta* **2010**, *55*, 6218–6227.

[41] C. Hsu, F. Mansfeld, *Corrosion* **2001**, *57*, 747–748.

[42] K. Szendrei, M. Speirs, W. Gomulya, D. Jarzab, M. Manca, O. V. Mikhnenko, M. Yarema, B. J. Kooi, W. Heiss, M. A. Loi, *Adv. Funct. Mater.* **2012**, *22*, 1598.

[43] S. M. Sze, K. K. Ng, *Physics of Semiconductor Devices*, Wiley, Hoboken, NJ, USA, **2007**.